Extended in-band and band-gap solutions of the nonlinear honeycomb lattice

E. Arévalo[1] and C. Mejía-Cortés[2]

[1]*Facultad de Física, Pontificia Universidad Católica de Chile, Casilla 306, Santiago, Chile*

[2]*Departamento de Física and MSI-Nucleus on Advanced Optics, Center for Optics and Photonics (CEFOP), Facultad de Ciencias, Universidad de Chile, Santiago, Chile*

(Received 1 May 2014; published 19 August 2014)

We study the dynamics of extended collective excitations in the pristine honeycomb lattice in the presence of the cubic nonlinearity. We show that not only band-gap excitations but also, stable and quasistable, extended excitations between the two lowest bands of the honeycomb system and labeled as in band exist. We also show that some solutions bifurcate from the saddle points of the Floquet band structure. Among other results, we report the existence of nontrivial stationary solutions even for the Floquet eigenvalue where the Dirac points occur. Numerical findings, in fair agreement with our theoretical predictions, are also reported.

DOI: 10.1103/PhysRevA.90.023835 PACS number(s): 42.65.Tg, 42.65.Wi, 42.82.Et

The research progress in a honeycomb system has been enormously stimulated by the great scientific and technological interest in carbon-based nanostructures, such as graphene [1,2]. Indeed, many exceptional properties observed in graphene are, in part, due to their natural honeycomb lattice (HL) structure. To mimic these properties, a variety of artificial HL systems have been experimentally realized and proposed as proxies for real graphene monolayers and ribbons [3–5]. For example, artificial HL systems offer a platform for studying massless Dirac quasiparticles and their phases [6–9].

One of the main characteristics of honeycomb systems is that the two lowest Floquet energy bands touch each other at certain isolated points called Dirac points (DPs). In pristine graphene the DPs energy level is called the Fermi level (FL). Due to the conical geometric shape of the lowest bands near the DPs, very high mobility has been predicted and observed in graphene and other honeycomb systems. In fact, high mobility is one the main characteristics of graphene [10–12]. However, for applications not only mobility, but also the absence of it is important. In this regard, several approaches to control mobility near the FL in graphene have been proposed and experimentally realized, namely, the use of external fields [10,13], disorder (Anderson localization) [14], modification of the band structure (e.g., by monolayer stretching, creation of multilayer graphene, creation of nanoribbons, or use of edge states) [15–18], and so on.

Low or zero mobility also are properties present naturally in pristine HL. Indeed, not only the lowest and highest points of the two lowest bands of honeycomb systems exhibit this property, but also the saddle points. However, in graphene the energy difference with respect to the FL of these points is too high for semiconductor applications. So, most of the research interest on monolayer graphene has been devoted to control electronic properties in the Dirac cones near to the FL.

In artificial HL, particularly in photonic systems, substantial effort has been directed towards realizing photonic arrays of coupled waveguides [19] that protect information transmission from diffraction [20] and/or disorder effects (due to random defects) [5,21]. For example, localized structures, called solitons and/or breathers with very low or nonmobility at the array transversal section, have been realized for this purpose [22]. These are nonlinear excitations that usually emerge as bifurcations from the lowest or highest points of the band structure into the band gaps [23–25]. In graphene systems the search for these kinds of excitations have attracted little attention due to the high-energy requirements (far from FL).

One important question that arises is whether in pristine HL systems, with nondistorted band structure, there might exist a scenario in which the absence of mobility near the DPs level appear. In graphene this scenario would correspond to energy values near the FL, where most of the relevant experiments are carried out.

Here we report a contraintuitive set of nonmobile extended solutions whose Floquet eigenvalues (quasi-energies) lie within the band-structure range in pristine nonlinear HL systems. Indeed, stable stationary nontrivial excitations are observed even at the DPs quasi-energy level (FL in condensed matter systems). This phenomenon is observed at the Γ point (position in the reciprocal-lattice space where the highest symmetry point of the band structure is located). In addition, at the M points (position of the saddle points of the band structure) we observe short-lived quasistable excitations.

To study the dynamics associated to the honeycomb geometry, we consider an array of evanescently coupled photonic waveguides with cubic nonlinear response. The array forms a two-dimensional (2D) pristine HL and we only consider interaction between nearest-neighbor interaction, as sketches Fig. 1(a). In the tight-binding approximation, the dynamics associated to the two lowest bands of the system is well described by a discrete nonlinear Schrödinger equation (NLSE) [26,27], reading as

$$i\,\partial_z \psi_{\mathbf{N}}(z) + C \sum_{\mathbf{N}' \neq \mathbf{N}} \psi_{\mathbf{N}'}(z) + U|\psi_{\mathbf{N}}(z)|^2 \psi_{\mathbf{N}}(z) = 0, \qquad (1)$$

where $\psi_{\mathbf{N}}$ is the complex amplitude of the electric field envelope function in the waveguide with index vector $\mathbf{N}$. The summation index vector $\mathbf{N}'$ in Eq. (1) runs over nearest-neighboring waveguides, C is the coupling constant between waveguides, and U is the cubic nonlinear coefficient. The discrete NLSE (1) is a generic equation that describes the dynamic associated to the two lowest bands of honeycomb arrays not only of coupled photonic waveguides [28], but also of Bose-Einstein condensates (BECs) trapped in deep optical HL [29]. For BECs the propagation coordinate z in Eq. (1) is interpreted as time. Several results (such as mobility [30], Zener transitions [18,31], Bloch oscillations [32],

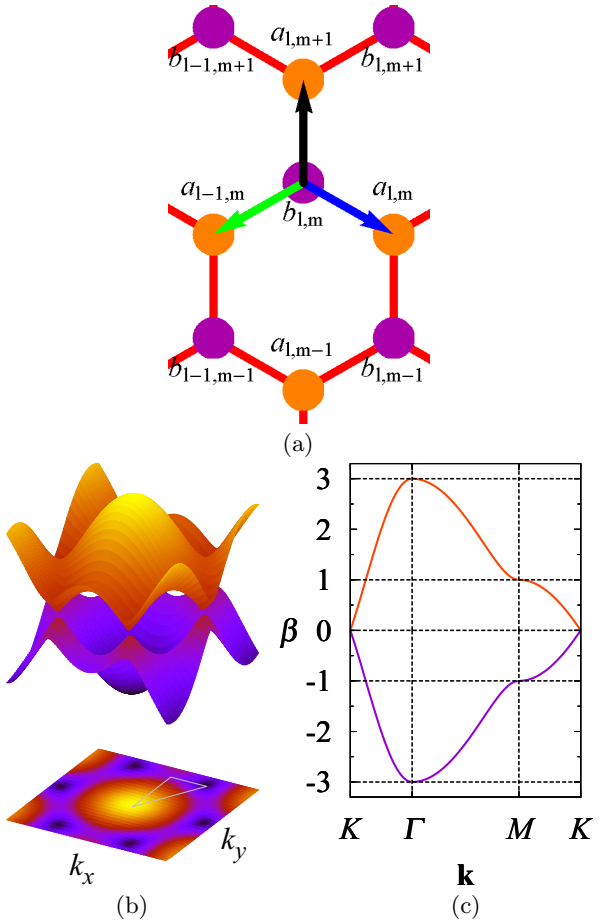

FIG. 1. (Color online) (a) Fraction of a HL showing the indexes of the sublattices and the displacement vectors $\vec{\delta}_0$ (black), $\vec{\delta}_1$ (blue), and $\vec{\delta}_2$ (green), respectively. (b) DPs connecting the two lowest bands of the HL sketched in (a). (c) Dispersion relation along the symmetry points in the HL.

Klein-tunneling [33], Berry phases [32], edge localization [34], and so on) from this equation and its continuous counterpart point to the fact that under some circumstances artificial systems may serve as proxies for studying electron behavior in graphene. It is important to note that the weakly cubic nonlinearity in Eq. (1) usually is neglected for electronic systems at low temperatures. However, this nonlinearity may appear due to phonon-electron interactions [35] arising from distortions of the lattice. In fact, a weakly cubic nonlinearity has been suggested to arise from adiabatic approximation in the Holstein formulation of graphene [30].

By using a Floquet ansatz of the form $\psi_{\mathbf{N}} = \exp(i\beta z)\eta_{\mathbf{N}}$ with $U = 0$, the linear spectrum of β (quasi-energies) can be obtained from Eq. (1) as a function of the Bloch wave vector $\mathbf{k}$ [see Fig. 1(b)]. Notice that in Eq. (1) the DPs level corresponds to $\beta = 0$. To determine the nonmobile extended solutions we substitute the Floquet ansatz into Eq. (1) and further use the Bloch ansatz $\eta_{\mathbf{N}} = \exp(i\mathbf{k}\cdot\mathbf{r}_{\mathbf{N}})\phi_{\mathbf{N}}$, where $\mathbf{r}_{\mathbf{N}}$ indicates the transverse position of the $\mathbf{N}$ waveguide. So the stationary equation for the $\phi_{\mathbf{N}}$ functions read as

$$\beta\phi_{\mathbf{N}} = C\sum_{\mathbf{N}'\neq\mathbf{N}} \phi_{\mathbf{N}'} e^{\mathbf{k}\cdot\boldsymbol{\delta}_{\mathbf{NN}'}} + U|\phi_{\mathbf{N}}|^2\phi_{\mathbf{N}}, \tag{2}$$

where $\boldsymbol{\delta}_{\mathbf{NN}'} = \mathbf{r}_{\mathbf{N}} - \mathbf{r}_{\mathbf{N}'}$ denotes the displacement vectors between the $\mathbf{N}$ and $\mathbf{N}'$ waveguides. For the sake of simplicity we chose $|\boldsymbol{\delta}_{\mathbf{NN}'}| = 1$. In Eq. (2), $\boldsymbol{\delta}_{\mathbf{NN}'}$ can take six forms, namely $\boldsymbol{\delta}_{\mathbf{NN}'} = \pm\boldsymbol{\delta}_0, \pm\boldsymbol{\delta}_1$, and $\pm\boldsymbol{\delta}_2$. In Fig. 1(a) these vectors are shown.

In nonlinear honeycomb systems, it has been shown that localized nonmobile solutions bifurcate from the lowest or highest points of the band structure [27], at $\mathbf{k} = (0,0)$ (Γ point). So far, it has been not known whether extended solutions exist at the HL Γ point. It is worth mentioning that extended solutions has been shown to exist in square lattices in the form of X waves [36,37], however, they are not expected to appear at the Γ point. On the other hand, the HL has two lowest bands, so its dynamics is expected to be different than that associated to the single band of the square lattices [38,39].

Extended nonmobile solutions at the Γ point can be obtained by imposing the value $\mathbf{k} = (0,0)$ and distinguishing between the two sublattice system in Eq. (2). For that we break the index-vector set $\{\mathbf{N}\}$ into two subsets, namely $\{\mathbf{N_A}\}$ and $\{\mathbf{N_B}\}$. Here $\mathbf{N_A} = (l,m+1)$ and $\mathbf{N_B} = (l,m)$ with $l \in \mathbb{Z}$ and $m \in \mathbb{Z}$ (mod 2).

Under these considerations, Eq. (2) takes the form

$$\begin{aligned} \beta a_{l,m+1} &= C(b_{l+1,m+1} + b_{l-1,m+1} + b_{l,m}) + U a_{l,m+1}^3, \\ \beta b_{l,m} &= C(a_{l+1,m} + a_{l-1,m} + a_{l,m+1}) + U b_{l,m}^3, \end{aligned} \tag{3}$$

where $a_{l,m+1} \equiv \phi_{\mathbf{N_A}}$ and $b_{l,m} \equiv \phi_{\mathbf{N_B}}$ are assumed to be real fields at the $\mathbf{N_A}$ and $\mathbf{N_B}$ sites, respectively. For extended solutions, we consider $a_{l',m'} = A$ and $b_{l'',m''} = B$ for all $(l',m') \in \{\mathbf{N_A}\}$ and $(l'',m'') \in \{\mathbf{N_B}\}$. Finally, it is straightforward to obtain coupled algebraic equations for A and B amplitudes from Eq. (3) and whose solutions are closed-form functions of β, C, and U constants.

A and B amplitudes versus β for focusing ($U > 0$) and defocusing ($U < 0$) nonlinearities at the Γ point are plotted in panels of Fig. 2. Solutions appear as branches that bifurcate from fold-bifurcation nodes. The bifurcation branches, which are sets of (β,A) or (β,B) points, open either to the right (focusing nonlinearity: $U > 0$) or to left

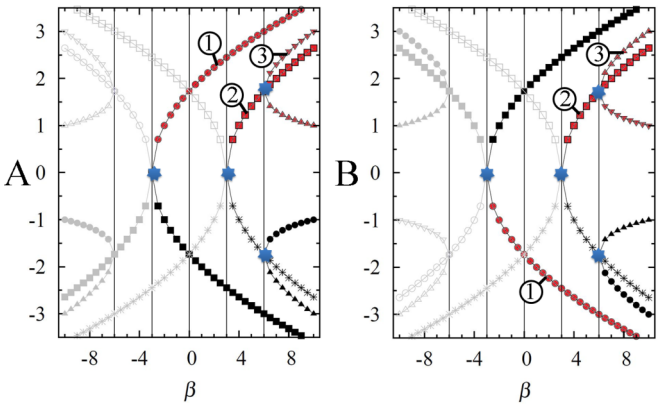

FIG. 2. (Color online) A and B amplitudes vs. β at the Γ point. Plot symbols indicate different solutions. Bifurcation branches opening to the right (left) correspond to the focusing (defocusing) nonlinearity. Blue stars indicate the position of the fold-bifurcation nodes in the focusing nonlinearity case.

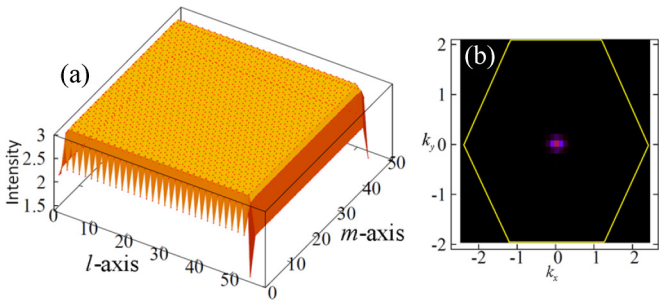

FIG. 3. (Color online) Intensity distribution for a solution with $\beta = 0$ in a 64×32 lattice size.

(defocusing nonlinearity: $U < 0$). Moreover, each bifurcation branch of the A amplitudes [Fig. 2(a)] is coupled to one bifurcation branch of the B amplitudes [Fig. 2(b)]. Related branches share the same plot symbols, as, e.g., circle branches labeled with ① in panels of Fig. 2 are coupled.

Let us have a closer look at the bifurcation branches labeled with ① in the panels of Fig. 2 for $U > 0$. The ①-branch range starts at the node in $\beta = -3$ (the lowest value of the band structure) and extends to $+\infty$, including the whole inner region ($-3 < \beta < 3$) between the two-band structure [see at the Γ point in Fig. 1(c)]. Usually in nonlinear systems, excitations with quasi-energies lying within the band region are labeled as in band [25,40,41]. In this regard, it has been believed from the theory of band-gap solitons that in-band excitations in honeycomb systems cannot exist [38] because the interband region is not a band gap, i.e., there is a band touching at the DPs [1,2]. However, as we show below, this is not the case. In fact, for nonlinear in-band excitations we observe three interesting β values: (i) $\beta \sim -3$ because the amplitude of the nonlinear solutions here can be infinitely small; (ii) $\beta = 0$ since solutions in this region lie exactly at the FL in condensed matter systems; and (iii) $\beta = 3$ because this value intersects the linear band structure, so the usual band-gap solitons [24,24,27] vanish here. However, we observe nontrivial stable solutions at this intersection. With respect to the external regions (i.e., $3 < \beta < \infty$ and $-\infty < \beta < -3$), they are semi-infinite band gaps, so excitations in these external regions can be labeled as band gap.

The solutions computed in Fig. 2 are infinitely extended, so they have to be truncated to fit finite-sized HLs (HL flakes). In this case the amplitude values at the sites in the HL-flake edges are estimated via a numerical analytic continuation method [42]. This method takes into account, as initial conditions, the amplitude solutions and quasi-energies plotted in Fig. 2 and can be used for any HL-flake shape. For simplicity, we have chosen rectangular HL flakes whose edge combines zigzag and armchair edges.

Figure 3(a) shows an example of a truncated intensity distribution calculated for $\beta = 0$ (FL in condensed matter systems) at the Γ point and associated to ① branches in Fig. 2. We observe that this intensity distribution is flat and only sites close to the edges present a different intensity values. In the reciprocal-lattice space this distribution is associated to a single Bloch mode at the Γ point, as shown in Fig. 3(b) where the effects from the lattice edges have been excluded. In fact, when performing the 2D Fourier transform of the excitation, a spatial 2D Gaussian filter has been used. In general, we observe that any nonlinear excitation associated to the ① branches look similar to that shown in Fig. 3(a), only their amplitude scale with β, as expected from the results shown in Fig. 2.

To study the behavior of the truncated solutions, we look at the evolution of the quasi-energy β during propagation. This can be estimated from the Floquet relation $\partial_z \psi_{l,m} = i\beta\psi_{l,m}$. So taking into account all sites of the lattice, it is straightforward to derive the expression

$$\beta = -\frac{i}{N_T} \sum_{l,m} \frac{\psi^{\star}_{l,m} \partial_z \psi_{l,m}}{|\psi_{l,m}|^2} \quad \text{for} \quad |\psi_{l,m}| \neq 0, \tag{4}$$

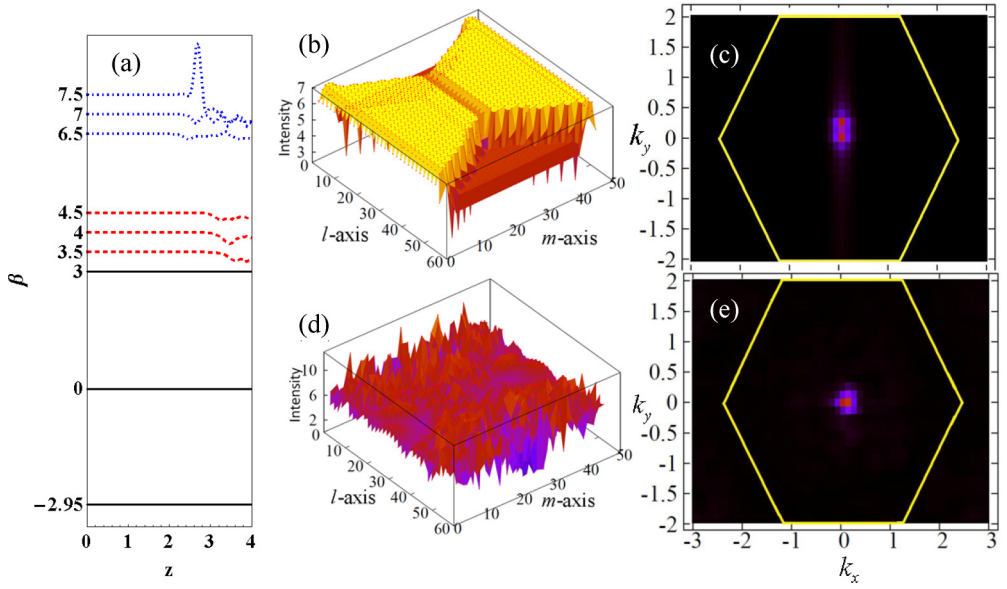

FIG. 4. (Color online) (a) Particular examples of β vs. z for amplitude solutions in Fig. (2): solid, dashed, and dotted lines correspond to the ①, ②, and ③ bifurcation branches, respectively. (b) Intensity distribution in the reciprocal lattice space (lines are drawn to show the edges of the first Brillouin zone).

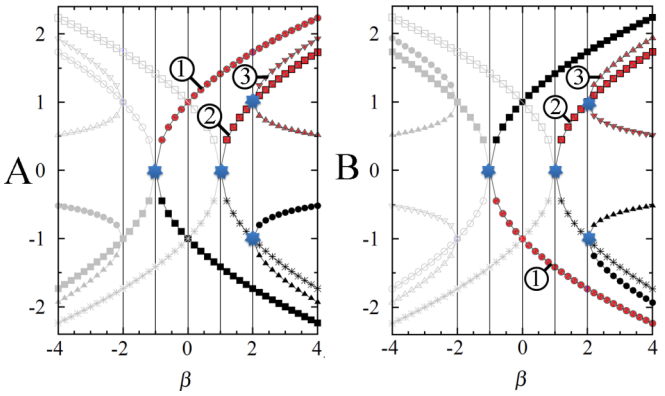

FIG. 5. (Color online) The same as Fig. 2 but for the M point.

where N_T is the total number of sites in the lattice and $\star$ indicates a complex conjugation.

Figure 4(a) shows several examples of the β evolution during propagation point for some solutions shown in Fig. 2. We observe that β remains constant for every solution associated with the ① branches (Fig. 2). In this case, stable stationary solutions are observed for very long distances ($z = 10^5$). For this distance a very small β variation (of the order of $\sim 5 \times 10^{-4}$) is observed. Figure 4(a) shows also a quasistationary behavior, i.e., β is constant for short initial distances ($z < 2$) and fluctuates for larger distances. This behavior belongs to solutions associated to the ② and ③ branches (Fig. 2). Snapshots of the intensity distribution for these short-lived excitations before and after instability arises are shown in Figs. 4(b) and 4(d), respectively. Figures 4(c) and 4(e) shows the respective distribution in the reciprocal-lattice space. This particular example corresponds to an excitation associated with the ② branches at $\beta = 4$ in Fig. 2. The initial intensity distribution in Fig. 4(b) presents a pattern that differs from the flat shape expected from amplitudes in Fig. 2. This pattern tends to lessen for very high β values (i.e., $\beta > 10$) and follows from the edges of the HL flake. In the reciprocal-lattice space [Fig. 4(c)], this initial pattern Fourier transforms into broad distribution around the Γ point, indicating the presence of several initial Bloch modes. During propagation a nonlinear modal interference causes the instability destroying [see Fig. 4(d)] the initial excitation shape. In the reciprocal lattice space [Fig. 4(e)] an irregular spot distribution around the Γ point is observed.

So far, we have discussed about solutions at the Γ point, however, in nonlinear square lattices, it has been shown that localized solitons can bifurcate from saddle points of the band structure [40]. So an open question here is whether for HL systems we can observe similar bifurcation at the M points. To solve this question, we chose one M point by imposing, for example, $\mathbf{k} = (0, 2\pi/3)$ in Eq. (2) to obtain

$$\begin{aligned} \beta\alpha_{l,m+1} &= C(b_{l+1,m+1} + b_{l-1,m+1} - b_{l,m}) + U\alpha_{l,m+1}^3, \\ \beta b_{l,m} &= C(\alpha_{l+1,m} + \alpha_{l-1,m} - \alpha_{l,m+1}) + U b_{l,m}^3, \end{aligned} \tag{5}$$

where $\alpha_{l,m+1} \equiv \phi_{\mathbf{N_A}} \exp(-i\pi/3)$ and $b_{l,m} \equiv \phi_{\mathbf{N_B}}$ are real fields at the $\mathbf{N_A}$ and $\mathbf{N_B}$ sites, respectively. Following the same procedure applied to the equations at the Γ point, we eventually obtain algebraic equations for the $A = \alpha_{l,m+1}$ and $B = b_{l,m}$ amplitudes, which are plotted as a function of β in Fig. 5. The behavior that we observe is similar to that plotted in Fig. 2. In fact, in Fig. 5, for focusing solutions ($U > 0$), bifurcation branches open from the nodes to the right. Besides, the lowest fold-bifurcation nodes lie exactly at $\beta = \pm 1$, which coincides with the position of the saddle points of the band structure. [see Fig. 1(c)]. Notice that the other fold-bifurcation nodes, at $\beta = \pm 2$ in Fig. 5, are effectively located outside of the band structure [see the M point in Fig. 1(c)] despite that these values lie within the global band range ($-3 \leqslant \beta \leqslant 3$).

For HL flakes, truncated stationary solutions are also estimated with the analytic-continuation method, taking into account amplitude solutions and quasi-energies plotted in Fig. 5. In Fig. 6(a), some examples of the β behavior along the propagation coordinate z are shown. For the ① and ② bifurcation branches in Fig. 5, truncated stationary solutions

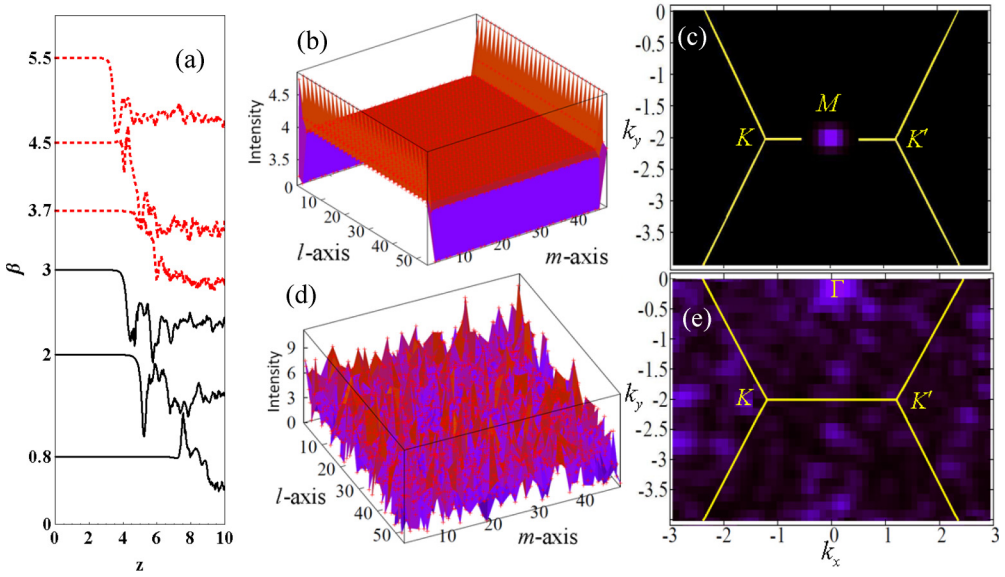

FIG. 6. (Color online) The same as Fig 4 but for the M point.

can be estimated for $\beta \gtrsim 0.8$ and $\beta \gtrsim 3.7$, respectively. No truncated stationary solution is found for ③ bifurcation branches. We observe in Fig. 6(a) that stationary solutions are in general short lived, i.e., after a short propagation distance the initial β value starts to fluctuate. This behavior occurs due to instabilities that arise at the lattice edges and eventually destroy the initial solution shape.

Figures 6(b) and 6(d) show snapshots of a truncated intensity distribution before and after the instability arises. The initial shape in Fig. 6(b) is associated to the ① bifurcation branch at $\beta = 3$ in Fig. 5. The initial excitation in the reciprocal-lattice space [Fig. 6(c)] is observed mostly as single Bloch mode at the M point that eventually, after instability arises, breaks and evolves into a noisy spot distribution at the Γ point. This phenomenology indicates that the lattice edges introduce Fourier components at the Γ point [not observed in Fig. 6(d) due to the imposed Gaussian filter] that eventually interferes with the Bloch mode at the M point destroying the initial distribution.

All in all, we have studied the behavior of extended nonlinear excitations in finite-shaped photonic honeycomb lattices. Several families of stable and quasistable in-band and band-gap excitations at the saddle points of the band structure have been found. Of particular interest are the stable in-band excitations since they can take any quasi-energy value within the linear band. Among other interesting results we show that nontrivial stable excitations at zero quasi-energy (Fermi level in condensed-matter systems) exist. The existence of these nontrivial excitations might hint at new schemes to achieve all-optical signal processing in photonic systems or, in the case of real monolayer graphene, to achieve new methods for controlling mobility near the Fermi level.

E.A. acknowledges funding support from FONDECYT Grant No. 1141223. C.M.-C. acknowledges funding support from FONDECYT Grant No. 3140608, Programa ICM P10-030-F, and PIA-CONICYT PFB0824.

[1] A. K. Geim and K. S. Novoselov, Nat. Mater. **6**, 183 (2007).
[2] A. H. Castro Neto, F. Guinea, N. M. R. Peres, K. S. Novoselov, and A. K. Geim, Rev. Mod. Phys. **81**, 109 (2009).
[3] M. Polini, F. Guinea, M. Lewenstein, H. C. Manoharan, and V. Pellegrini, Nat. Nanotechnol. **8**, 625 (2013).
[4] L. Nádvorník, M. Orlita, N. A. Goncharuk, L. Smrčka, V. Novák, V. Jurka, K. Hruška, Z. Výborný, Z. R. Wasilewski, M. Potemski *et al.*, New J. Phys. **14**, 053002 (2012).
[5] M. C. Rechtsman, J. M. Zeuner, Y. Plotnik, Y. Lumer, D. Podolsky, F. Dreisow, S. Nolte, M. Segev, and A. Szameit, Nature (London) **496**, 196 (2013).
[6] K. L. Lee, B. Grémaud, R. Han, B.-G. Englert, and C. Miniatura, Phys. Rev. A **80**, 043411 (2009).
[7] P. Soltan-Panahi, D.-S. Luhmann, J. Struck, P. Windpassinger, and K. Sengstock, Nat. Phys. **8**, 71 (2012).
[8] A. Bostwick, T. Ohta, T. Seyller, K. Horn, and E. Rotenberg, Nat. Phys. **3**, 36 (2006).
[9] M. Syafwan, H. Susanto, S. M. Cox, and B. A. Malomed, J. Phys. A: Math. Theor. **45**, 075207 (2012).
[10] K. S. Novoselov, A. K. Geim, S. V. Morozov, D. Jiang, Y. Zhang, S. V. Dubonos, I. V. Grigorieva, and A. A. Firsov, Science **306**, 666 (2004).
[11] E. H. Hwang, S. Adam, and S. Das Sarma, Phys. Rev. Lett. **98**, 186806 (2007).
[12] K. Bolotin, K. Sikes, Z. Jiang, M. Klima, G. Fudenberg, J. Hone, P. Kim, and H. Stormer, Solid State Commun. **146**, 351 (2008).
[13] T. Oka and H. Aoki, Phys. Rev. B **79**, 081406 (2009).
[14] M. Y. Han, J. C. Brant, and P. Kim, Phys. Rev. Lett. **104**, 056801 (2010).
[15] M. Y. Han, B. Özyilmaz, Y. Zhang, and P. Kim, Phys. Rev. Lett. **98**, 206805 (2007).
[16] Y.-W. Son, M. L. Cohen, and S. G. Louie, Phys. Rev. Lett. **97**, 216803 (2006).
[17] V. M. Pereira and A. H. Castro Neto, Phys. Rev. Lett. **103**, 046801 (2009).
[18] E. Arévalo and L. Morales-Molina, Europhys. Lett. **96**, 60011 (2011).
[19] M. C. Rechtsman, Y. Plotnik, J. M. Zeuner, D. Song, Z. Chen, A. Szameit, and M. Segev, Phys. Rev. Lett. **111**, 103901 (2013).
[20] K. J. H. Law, H. Susanto, and P. G. Kevrekidis, Phys. Rev. A **78**, 033802 (2008).
[21] J. M. Zeuner, M. C. Rechtsman, S. Nolte, and A. Szameit, Opt. Lett. **39**, 602 (2014).
[22] L. Q. English, F. Palmero, J. F. Stormes, J. Cuevas, R. Carretero-González, and P. G. Kevrekidis, Phys. Rev. E **88**, 022912 (2013).
[23] P. G. Kevrekidis, K. O. Rasmussen, and A. R. Bishop, Phys. Rev. E **61**, 2006 (2000).
[24] R. A. Vicencio and M. Johansson, Phys. Rev. A **87**, 061803 (2013).
[25] J. Zeng and B. A. Malomed, J. Opt. Soc. Am. B **30**, 1786 (2013).
[26] F. Lederer, G. I. Stegeman, D. N. Christodoulides, G. Assanto, M. Segev, and Y. Silberberg, Phys. Rep. **463**, 1 (2008).
[27] M. I. Molina and Y. S. Kivshar, Opt. Lett. **35**, 2895 (2010).
[28] M. J. Ablowitz, S. D. Nixon, and Y. Zhu, Phys. Rev. A **79**, 053830 (2009).
[29] L. Haddad and L. Carr, Phys. D (Amsterdam, Neth.) **238**, 1413 (2009).
[30] W. S. Dias, M. L. Lyra, and F. A. B. F. de Moura, Phys. Rev. B **82**, 233102 (2010).
[31] V. S. Shchesnovich, A. S. Desyatnikov, and Y. S. Kivshar, Opt. Express **16**, 14076 (2008).
[32] H. Trompeter, W. Krolikowski, D. N. Neshev, A. S. Desyatnikov, A. A. Sukhorukov, Y. S. Kivshar, T. Pertsch, U. Peschel, and F. Lederer, Phys. Rev. Lett. **96**, 053903 (2006).
[33] O. Bahat-Treidel, O. Peleg, M. Grobman, N. Shapira, M. Segev, and T. Pereg-Barnea, Phys. Rev. Lett. **104**, 063901 (2010).
[34] M. J. Ablowitz, C. W. Curtis, and Y. Zhu, Phys. Rev. A **88**, 013850 (2013).
[35] G. Kalosakas, S. Aubry, and G. P. Tsironis, Phys. Rev. B **58**, 3094 (1998).
[36] E. Arévalo, Phys. Rev. A **86**, 053829 (2012).

[37] Q. E. Hoq, J. Gagnon, P. G. Kevrekidis, B. A. Malomed, D. J. Frantzeskakis, and R. Carretero-González, Mathematics and Computers in Simulation **80**, 721 (2009).
[38] O. Peleg, G. Bartal, B. Freedman, O. Manela, M. Segev, and D. N. Christodoulides, Phys. Rev. Lett. **98**, 103901 (2007).
[39] E. Arévalo, Phys. Rev. Lett. **102**, 224102 (2009).
[40] X. Wang, Z. Chen, J. Wang, and J. Yang, Phys. Rev. Lett. **99**, 243901 (2007).
[41] J. Yang, Phys. Rev. A **82**, 053828 (2010).
[42] L. D. G. Sigalotti and O. Rendn, Chaos, Solitons Fractals **32**, 1611 (2007).